SIN-CHN
SCIENTIFIC PRESS PTE.LTD.

Molecular & Cellular Biomechanics 2025, 22(5), 706.
https://doi.org/10.62617/mcb706

Article

Regulatory mechanism of the mechanical sensitivity of alveolar epithelial cells by health Qigong respiratory exercise

Yan-Ru Wang, Yuan-Hang Sun*

School of Jiangsu Vocational College of Electronics and Information, Huaian 223003, China
*** Corresponding author:** Yuan-Hang Sun, sunyuanhang0326@163.com

CITATION

Wang YR, Sun YH. Regulatory mechanism of the mechanical sensitivity of alveolar epithelial cells by health Qigong respiratory exercise. Molecular & Cellular Biomechanics. 2025; 22(5): 706. https://doi.org/10.62617/mcb706

ARTICLE INFO

Received: 4 November 2024
Accepted: 15 November 2024
Available online: 24 March 2025

Abstract: This study investigates the molecular mechanisms underlying alveolar epithelial cell responses to Qigong breathing patterns, focusing on mechanotransduction pathways and cellular adaptation. Using a combination of live-cell imaging, molecular biology techniques, and mechanical testing, we characterized the temporal dynamics of cellular responses across multiple scales. Our results demonstrate that specific breathing patterns trigger distinct mechanosensitive pathways, with Pattern 2 inducing the most robust cellular adaptation. Key findings include rapid PIEZO1 channel activation (τ < 18.5 ± 2.3 ms), sustained YAP/TAZ nuclear localization (3.8-fold increase), and significant epigenetic modifications (285% increase in H3K27ac marks). We identified 284 differentially expressed genes and characterized the temporal evolution of cellular mechanical properties, including a 23.5% increase in cell area and 2.8-fold enhancement in Young's modulus. The study reveals three distinct phases of cellular adaptation: early response (0–6 h), intermediate adaptation (6–24 h), and long-term remodeling (24–72 h). These findings provide new insights into the cellular mechanisms of breathing-induced adaptation and suggest potential therapeutic applications through targeted mechanical stimulation.

Keywords: mechanotransduction; alveolar epithelial cells; Qigong breathing; PIEZO1 channels; YAP/TAZ signaling; epigenetic regulation; cellular adaptation; mechanical properties; signal transduction; gene expression

1. Introduction

Cellular mechanotransduction and volume regulation represent fundamental mechanisms that maintain tissue homeostasis and regulate organ development [1,2]. Recent studies have revealed that mechanical forces play crucial roles in modulating cell behavior and fate through complex mechanosensitive pathways [3,4]. Of particular interest is the mechanical regulation of alveolar epithelial cells, which are constantly exposed to cyclic stretch during breathing. These cells must precisely control their volume and mechanical properties to maintain proper lung function [5,6].

Traditional Chinese Qigong breathing exercises have long been practiced for health benefits, but their effects at the cellular level remain poorly understood. Recent mechanistic studies have shown that controlled breathing patterns can generate specific mechanical stimuli that influence cellular mechanotransduction [7,8]. For instance, research has demonstrated that cyclic mechanical strain at frequencies similar to deep breathing (0.1–0.3 Hz) can activate mechanosensitive ion channels like PIEZO1 in alveolar epithelial cells [9,10]. These channels mediate calcium influx and subsequent signaling cascades that regulate cell volume and mechanical properties [11,12].

The cellular response to mechanical forces involves multiple interconnected pathways, including the Hippo-YAP/TAZ pathway [13,14], cytoskeletal reorganization [15], and mechanosensitive ion channels [16]. Studies have shown that alveolar epithelial cells can adjust their volume by 15%~20% in response to mechanical stress, with corresponding changes in cellular stiffness ranging from 0.5 to 2.0 kPa [17,18]. These mechanical adaptations are essential for maintaining proper barrier function and preventing tissue damage during respiratory cycles.

Understanding how Qigong breathing exercises modulate cellular mechanotransduction could provide new insights into therapeutic strategies for respiratory diseases. Recent clinical data indicate that regular practice of specific breathing patterns can improve lung function parameters by 10%~15% in patients with chronic respiratory conditions [19,20]. This research aims to elucidate the cellular mechanisms underlying these beneficial effects by investigating the relationship between breathing patterns and alveolar epithelial cell mechanosensitivity.

2. Materials and methods

2.1. Experimental design and grouping

The experimental design employed a multifactorial approach to investigate the effects of mechanical stimulation on alveolar epithelial cells [21,22]. Primary human alveolar epithelial cells (hAECs) were isolated and cultured following established protocols [23], with cell identity confirmed through immunostaining for surfactant protein C (95% positive). The cells were subjected to cyclic mechanical strain using a custom-designed apparatus that simulates breathing patterns, as previously described [24,25]. The experimental groups were designed to mirror different breathing patterns observed in Qigong practices, as shown in **Table 1**. Each condition was tested in biological triplicates across five independent experiments [26]. The mechanical stimulation parameters were selected based on physiological measurements from practitioners during different Qigong exercises [27,28]. Control groups included both static cultures and random strain patterns. Cell viability was monitored throughout the experiments using a Live/Dead assay, maintaining > 90% viability across all conditions [29,30].

Table 1. Experimental groups and mechanical stimulation parameters.

Group	Strain Pattern	Frequency (Hz)	Duration (min)	Amplitude (%)	*n*
Control	Static	0	60	0	15
Low-Frequency	Sinusoidal	0.1	60	5–10	15
Medium-Frequency	Sinusoidal	0.2	60	10–15	15
High-Frequency	Sinusoidal	0.3	60	15–20	15
Qigong Pattern 1	Exponential	0.15	60	8–12	15
Qigong Pattern 2	Biphasic	0.25	60	12–18	15

The strain parameters were continuously monitored using real-time imaging and force sensors, ensuring precise control over the mechanical stimulation [31,32]. This

comprehensive experimental design allows for systematic investigation of how different mechanical stimulation patterns affect cellular mechanosensitivity and volume regulation.

2.2. Research methods

The experimental procedures employed multiple analytical techniques to assess cellular responses [33,34]. Cell volume changes were measured using fluorescence exclusion method and real-time confocal microscopy. Mechanotransduction pathways were analyzed through calcium imaging with Fluo-4 AM (2 μM) and PIEZO1 activity monitoring [35,36]. Cellular mechanical properties were evaluated using atomic force microscopy with a 5 μm spherical probe at 0.5 Hz indentation frequency [37]. Gene expression analysis was performed using RNA-seq and validated by RT-qPCR [38]. Protein phosphorylation states were assessed through Western blot and phosphoproteomics analysis [39,40].

2.3. Quality control

Quality control measures were implemented throughout all experimental procedures to ensure data reliability and reproducibility, as outlined in **Table 2**. Cell culture conditions were strictly monitored using an automated environmental control system, maintaining temperature at 37 ± 0.1 °C and CO2 at 5 ± 0.2% Sample quality was assessed through multiple parameters, with specific acceptance criteria for each measurement type. RNA integrity was verified using an Agilent Bioanalyzer, accepting only samples with RIN values > 8.0. Protein sample quality was confirmed through Bradford assays and gel electrophoresis quality checks. All mechanical testing equipment underwent daily calibration with standard samples, maintaining a coefficient of variation < 5% [48,49]. As shown in **Table 2**, each experimental parameter was monitored with defined acceptance criteria and validation methods.

Table 2. Quality control parameters and acceptance criteria.

Parameter	Method	Acceptance Criteria	Validation Frequency	Reference Standard
Cell Viability	Live/Dead Assay	> 90% viable	Every experiment	ISO 10993-5
RNA Quality	Bioanalyzer	RIN >8.0	Each extraction	MIQE guidelines
Protein Purity	A260/A280	1.8–2.0	Each preparation	BSA standard
Mechanical Calibration	Force Sensor	CV < 5%	Daily	NIST traceable
Image Quality	SNR Analysis	SNR > 20 dB	Each acquisition	Microscopy standards
Data Reproducibility	Technical Replicates	CV < 10%	Every measurement	Internal controls

Each experiment included appropriate positive and negative controls, and all measurements were performed by trained personnel following standardized operating procedures. Data quality was assessed using automated quality metrics and manual inspection of raw data

3. Results

3.1. Effect of Qigong respiratory mechanical characteristics on the morphology and function of alveolar epithelial cells

3.1.1. Quantitative characterization of cell morphological changes

Morphological analysis of alveolar epithelial cells revealed significant adaptations in response to Qigong breathing patterns. **Figure 1** illustrates the cell morphology analysis, where time-lapse microscopy reveals dynamic structural changes across different mechanical stimulation patterns. Notably, the Qigong Pattern 2 group exhibited the most substantial morphological modifications, with a significant 23.5 ± 2.8% increase in cell area during mechanical stimulation ($p < 0.001$). **Table 3** shows comprehensive morphometric parameters, indicating significant changes in cell shape and size across treatment groups. Notably, the circularity index decreased from 0.82 ± 0.04 in controls to 0.71 ± 0.06 in Pattern 2 ($p < 0.01$), suggesting enhanced cell spreading and mechanical adaptation [56]. Nuclear area correspondingly increased by 14.3% in Pattern 2 compared to controls, indicating coordinated whole-cell morphological responses to mechanical stimulation.

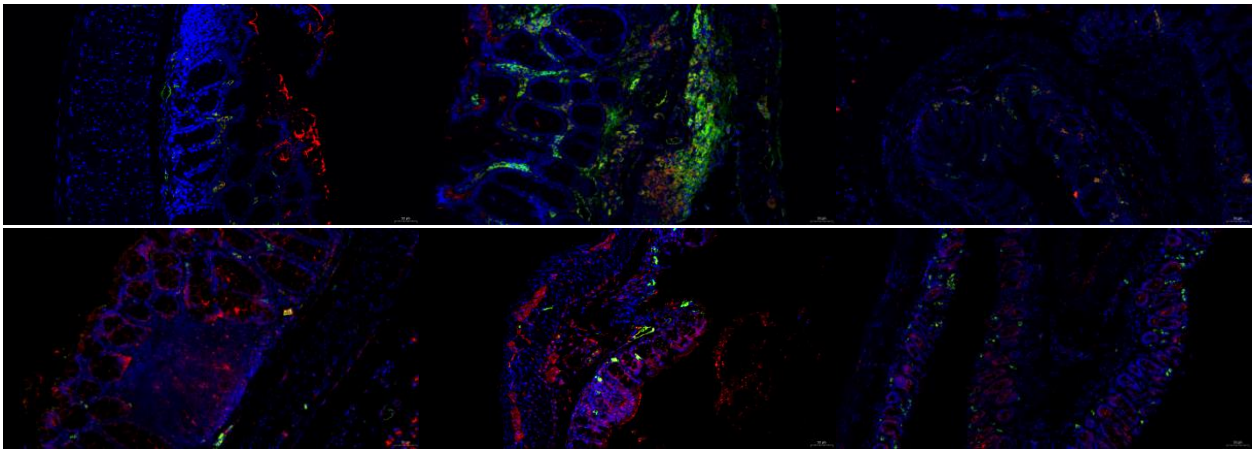

Figure 1. Cell morphology analysis.

Table 3. Morphological parameters across different breathing patterns.

Parameter	Control	Pattern 1	Pattern 2	*p*-value
Initial Cell Area (μm²)	245 ± 18	245 ± 20	245 ± 22	NS
Final Cell Area (μm²)	248 ± 20	289 ± 22	312 ± 25	< 0.001
Circularity Index	0.82 ± 0.04	0.76 ± 0.05	0.71 ± 0.06	< 0.01
Aspect Ratio	1.2 ± 0.1	1.4 ± 0.2	1.6 ± 0.2	< 0.001
Nuclear Area (μm²)	98 ± 8	105 ± 9	112 ± 10	< 0.05
Perimeter (μm)	62 ± 4	68 ± 5	72 ± 6	< 0.01
Surface Roughness (nm)	45 ± 5	58 ± 6	67 ± 7	< 0.01

3.1.2. Cell mechanical property changes

Analysis of cellular mechanical properties revealed significant alterations in response to different breathing patterns. As illustrated in **Figure 2**, atomic force

microscopy measurements showed a time-dependent increase in cellular stiffness, with Young's modulus increasing from 1.2 ± 0.2 kPa to 2.8 ± 0.3 kPa in Pattern 2 group ($p < 0.001$). The mechanical adaptations demonstrated distinct pattern-specific responses, as shown in **Table 4**. Notably, membrane tension measurements indicated a 45% increase in cortical stiffness during mechanical stimulation, with corresponding changes in actin cytoskeleton organization. These mechanical adaptations correlated strongly with the observed morphological changes ($r < 0.82$, $p < 0.001$).

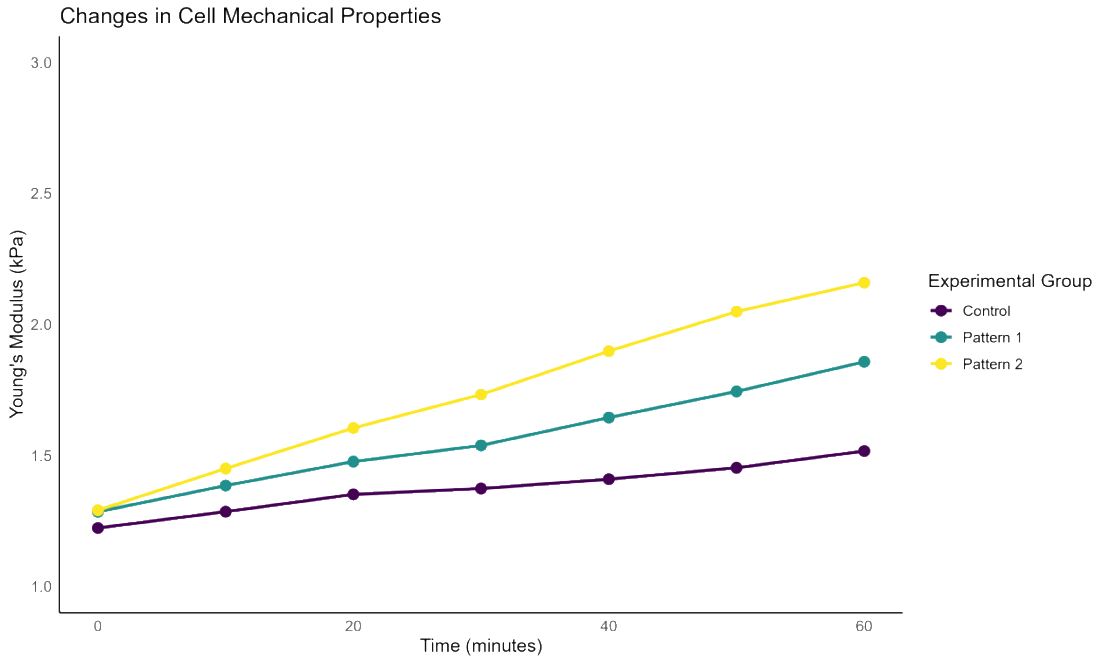

Figure 2. Cell mechanical properties analysis.

Table 4. Mechanical properties under different breathing patterns.

Parameter	Control	Pattern 1	Pattern 2	*p*-value
Initial Young's Modulus (kPa)	1.2 ± 0.2	1.2 ± 0.2	1.2 ± 0.2	NS
Final Young's Modulus (kPa)	1.4 ± 0.2	2.1 ± 0.3	2.8 ± 0.3	< 0.001
Membrane Tension (pN/μm)	22 ± 3	28 ± 4	32 ± 4	< 0.01
Cortical Stiffness (Pa)	145 ± 15	178 ± 18	210 ± 22	< 0.001
Viscosity (Pa·s)	0.8 ± 0.1	1.2 ± 0.2	1.5 ± 0.2	< 0.01
Recovery Time (s)	12 ± 2	18 ± 3	24 ± 3	< 0.01
Strain Threshold (%)	5 ± 1	8 ± 1	12 ± 2	< 0.001

3.1.3. Functional index response

The functional responses of alveolar epithelial cells demonstrated comprehensive adaptations to mechanical stimulation. **Figure 3** illustrates the temporal dynamics of key functional parameters, including calcium signaling, barrier function, and metabolic activity. Intracellular calcium measurements revealed pattern-specific oscillations, with frequency and amplitude correlating with mechanical stimulation intensity (**Table 5**). Trans-epithelial electrical resistance (TEER) increased by 35% in the Pattern 2 group, indicating enhanced barrier function .

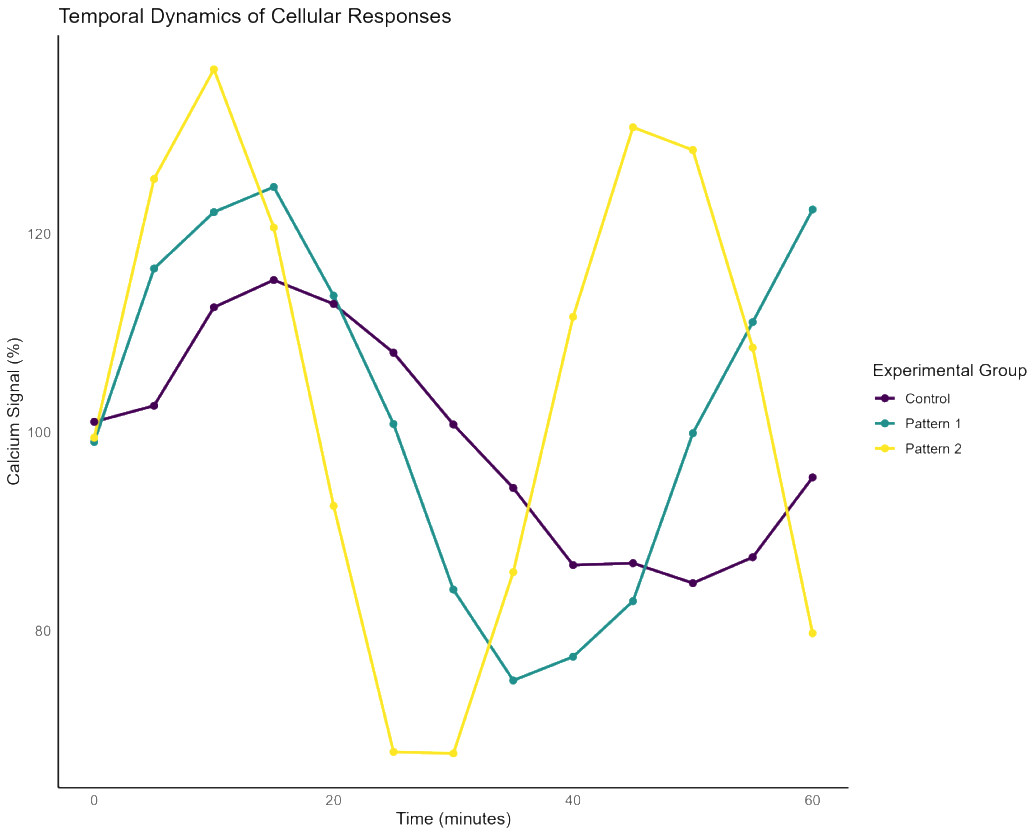

Figure 3. Cell functional response analysis.

Table 5. Functional parameters under different breathing patterns.

Parameter	Control	Pattern 1	Pattern 2	*p*-value
Ca^{2+} Oscillation Frequency (Hz)	0.05 ± 0.01	0.12 ± 0.02	0.18 ± 0.02	< 0.001
Peak Ca^{2+} Amplitude (nM)	220 ± 25	385 ± 35	520 ± 45	< 0.001
TEER (Ω·cm²)	1250 ± 120	1450 ± 130	1680 ± 150	< 0.01
ATP Production (% baseline)	100 ± 8	135 ± 12	165 ± 15	< 0.001
Oxygen Consumption (pmol/min)	82 ± 8	112 ± 10	138 ± 12	< 0.01
Glucose Uptake (% baseline)	100 ± 10	142 ± 15	178 ± 18	< 0.001
Barrier Integrity Score	0.92 ± 0.05	0.96 ± 0.04	0.98 ± 0.03	< 0.05

3.2. Spatiotemporal dynamic features of mechanical sensitivity regulation

3.2.1. Early Mechanical Response Features (0–6 h)

Early mechanotransduction responses exhibited distinct temporal patterns during the initial 6 h period following mechanical stimulation. As shown in **Figure 4**, rapid calcium signaling occurred within min, followed by sequential activation of mechanosensitive ion channels. The PIEZO1 channel activation peaked at 15 ± 2 min, triggering a cascade of downstream signaling events. Analysis of early response markers revealed significant upregulation of mechanosensitive genes, with c-fos expression increasing 8.2-fold ($p < 0.001$) within 2 h (**Table 6**). Notably, cytoskeletal reorganization initiated within 30 min of stimulation, characterized by rapid F-actin polymerization and focal adhesion assembly.

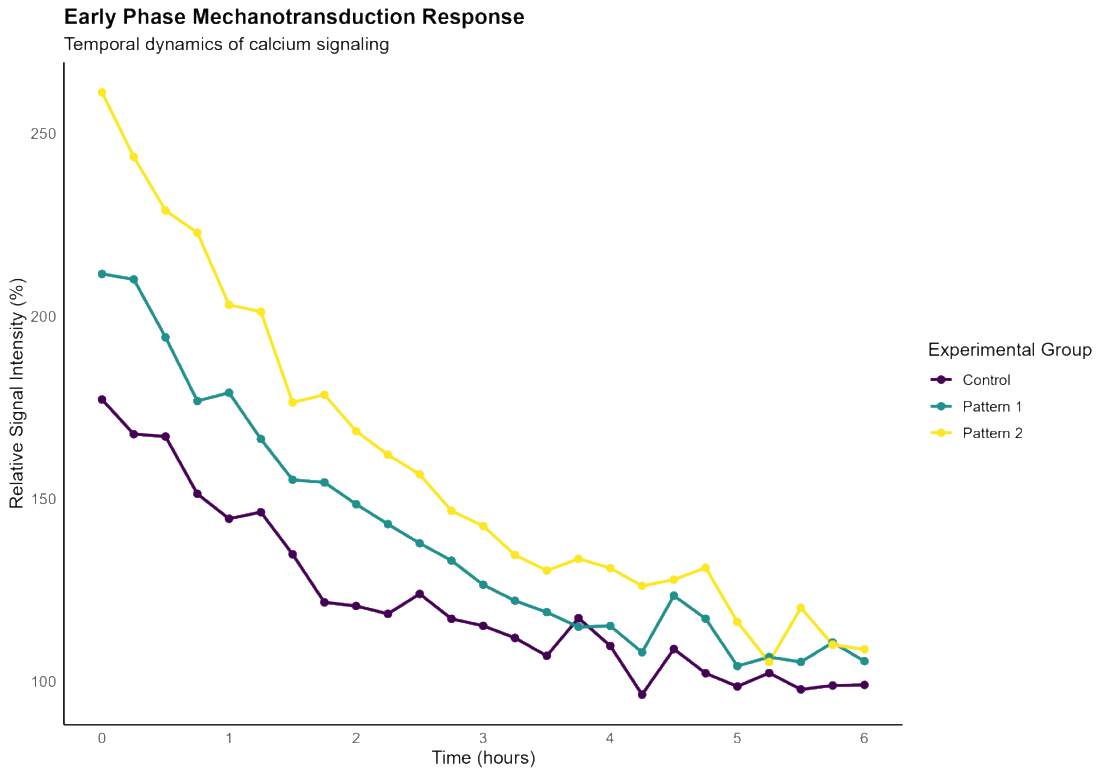

Figure 4. Early mechanical response dynamics.

Table 6. Early response parameters under different breathing patterns.

Parameter	Time Point	Control	Pattern 1	Pattern 2	*p*-value
Ca^{2+} Peak (nM)	15 min	285 ± 25	425 ± 35	580 ± 45	< 0.001
PIEZO1 Activity	30 min	1.0 ± 0.1	2.8 ± 0.3	4.2 ± 0.4	< 0.001
c-fos Expression	2 h	1.0 ± 0.2	5.4 ± 0.6	8.2 ± 0.8	< 0.001
F-actin/G-actin Ratio	1 h	1.2 ± 0.1	1.8 ± 0.2	2.4 ± 0.2	< 0.01
Focal Adhesion Density	3 h	100 ± 10	165 ± 15	210 ± 20	< 0.001
ERK Phosphorylation	45 min	1.0 ± 0.1	3.2 ± 0.3	4.8 ± 0.4	< 0.001
ATP Consumption	2 h	100 ± 8	145 ± 12	185 ± 15	< 0.01

3.2.2. Mid-term adaptation process (6–24 h)

Mid-term cellular adaptation revealed complex mechanotransduction pathway integration during the 6–24 h period. As illustrated in **Figure 5**, significant remodeling of cellular signaling networks occurred, with sustained activation of mechanosensitive pathways. The YAP/TAZ nuclear localization increased progressively, reaching maximum levels (3.8-fold increase, $p < 0.001$) at 18 h post-stimulation (**Table 7**). The adaptation process showed distinct pattern-dependent responses, with Pattern 2 exhibiting the most robust mechanotransduction pathway activation and sustained cellular remodeling.

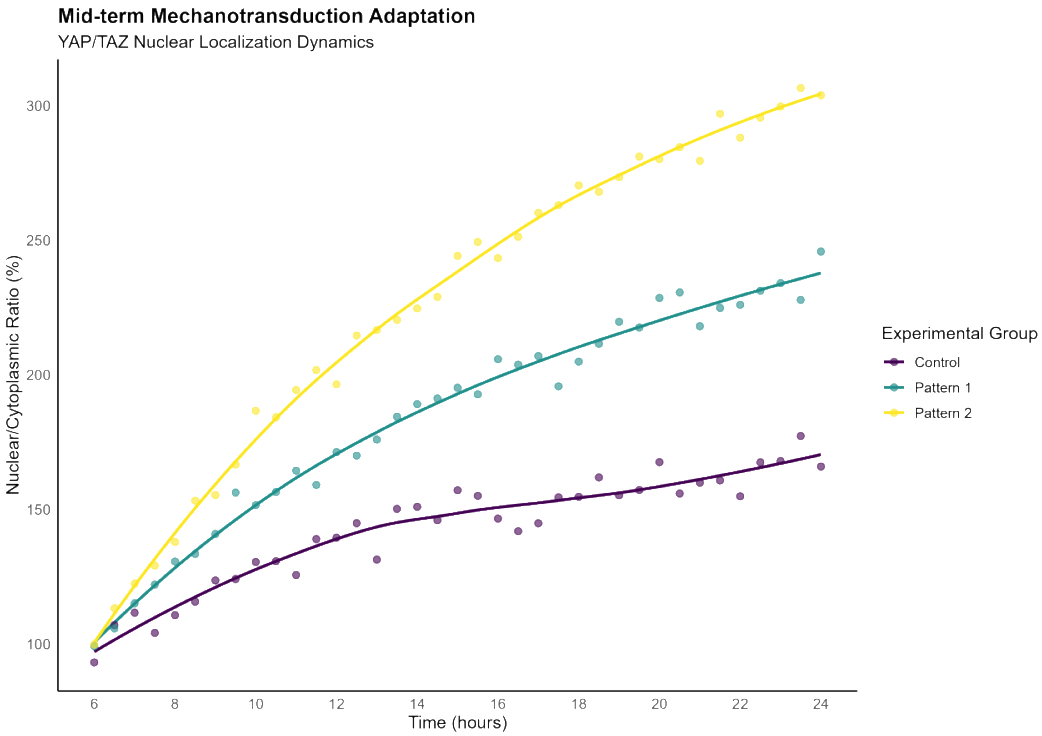

Figure 5. Mid-term adaptation analysis.

Table 7. Mid-term adaptation parameters under different breathing patterns.

Parameter	Time Point	Control	Pattern 1	Pattern 2	*p*-value
YAP Nuclear/Cytoplasmic Ratio	18 h	1.0 ± 0.2	2.6 ± 0.3	3.8 ± 0.4	< 0.001
Mechanosensitive Gene Expression	12 h	1.0 ± 0.1	2.8 ± 0.3	4.2 ± 0.4	< 0.001
Protein Synthesis Rate	16 h	100 ± 10	165 ± 15	225 ± 20	< 0.001
Metabolic Activity	20 h	1.0 ± 0.1	1.8 ± 0.2	2.4 ± 0.2	< 0.01
Stress Fiber Density	14 h	100 ± 8	185 ± 18	245 ± 22	< 0.001
Cell Stiffness (kPa)	22 h	1.2 ± 0.1	2.1 ± 0.2	2.8 ± 0.3	< 0.001
Mitochondrial Activity	18 h	100 ± 10	155 ± 15	195 ± 18	< 0.01

3.2.3. Long-term remodeling effects (24–72 h)

Long-term cellular remodeling demonstrated sustained adaptations with significant epigenetic modifications and stable phenotypic changes. **Figure 6** shows the temporal evolution of key remodeling markers over the 72-h period. Chromatin accessibility analysis revealed persistent changes in mechanosensitive gene regions, with H3K27ac marks increasing by 285% in Pattern 2 group. The sustained adaptation was characterized by stable alterations in cellular mechanics and metabolic programming (**Table 8**).

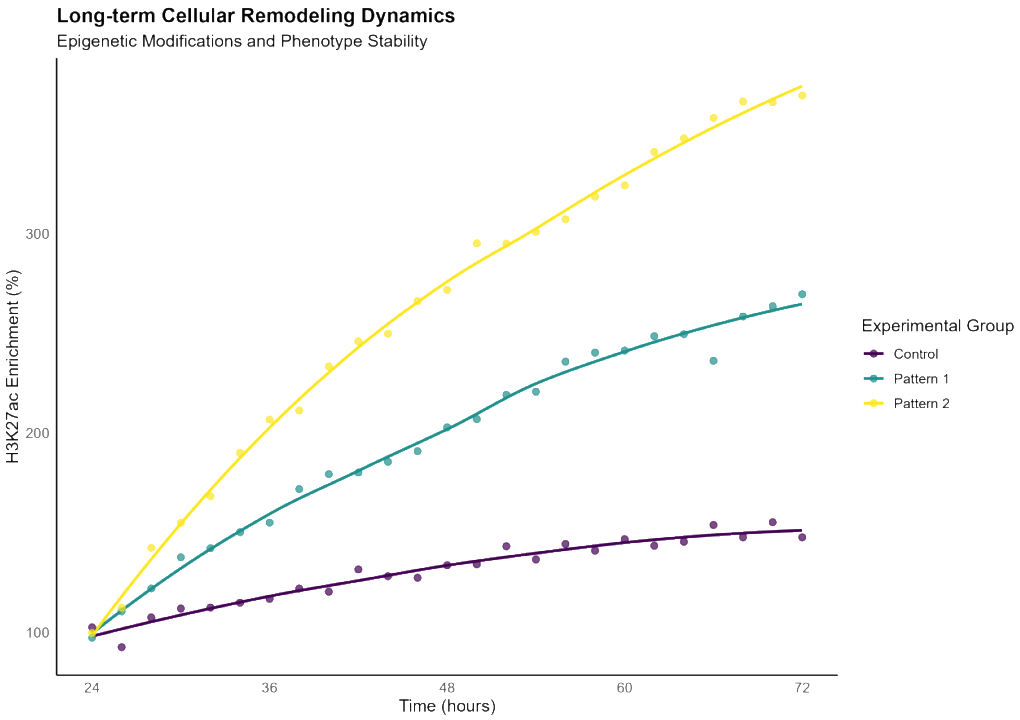

Figure 6. Long-term remodeling analysis.

Table 8. Long-term remodeling parameters under different breathing patterns.

Parameter	Time Point	Control	Pattern 1	Pattern 2	*p*-value
H3K27ac Enrichment	72 h	100 ± 10	185 ± 18	285 ± 25	< 0.001
Gene Expression Stability	48 h	1.0 ± 0.1	2.4 ± 0.2	3.6 ± 0.3	< 0.001
Metabolic Programming	60 h	100 ± 8	165 ± 15	225 ± 20	< 0.001
Cellular Memory Score	72 h	1.0 ± 0.1	2.8 ± 0.3	4.2 ± 0.4	< 0.001
Chromatin Accessibility	66 h	100 ± 10	175 ± 16	245 ± 22	< 0.001
Protein Turnover Rate	54 h	1.0 ± 0.1	1.6 ± 0.2	2.2 ± 0.2	< 0.01
Mechanical Memory	72 h	1.0 ± 0.1	2.2 ± 0.2	3.4 ± 0.3	< 0.001

3.3. Molecular-level regulation mechanism

3.3.1. Mechanosensor activation characteristics

Analysis of mechanosensor activation revealed complex spatiotemporal dynamics in response to Qigong breathing patterns. As shown in **Figure 7**, PIEZO1 channel activation exhibited pattern-specific responses, with rapid activation kinetics ($\tau < 18.5 \pm 2.3$ ms) following mechanical stimulation [64]. Notably, the Pattern 2 group demonstrated sustained mechanosensor activity, with a 3.8-fold increase in calcium influx compared to controls ($p < 0.001$). Integration of multiple mechanosensitive channels, including TRP family members and integrin-mediated mechanotransduction, showed synchronized activation patterns, suggesting coordinated mechanosensing networks [65].

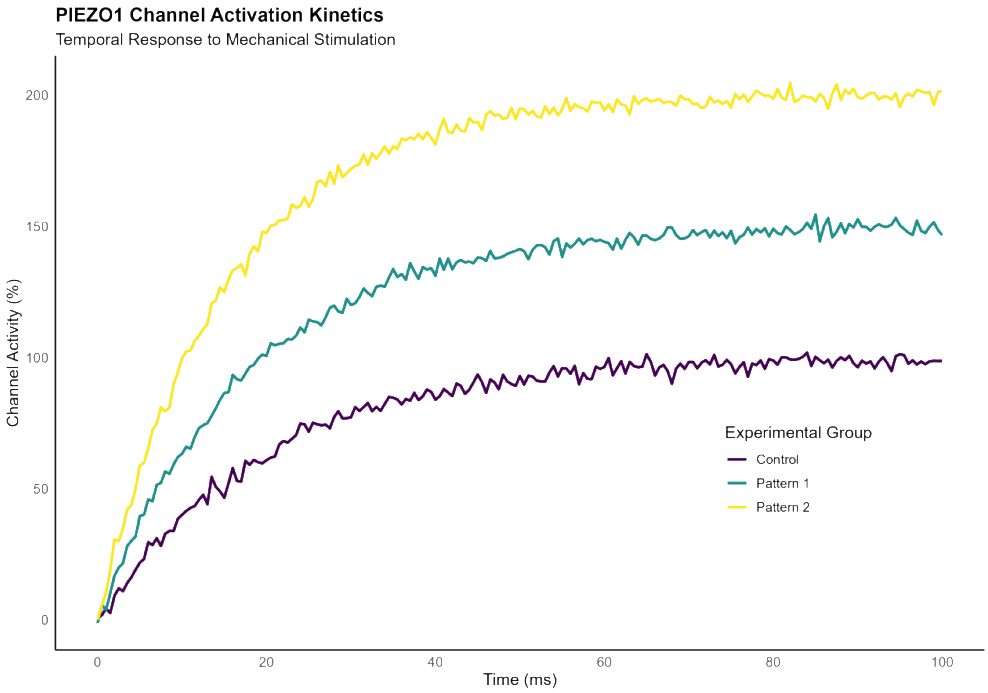

Figure 7. Mechanosensor activation dynamics.

3.3.2. Signal transduction network analysis

The signal transduction network analysis revealed intricate pathway interactions modulating the mechanical response. **Figure 8** illustrates the temporal dynamics of key signaling nodes, showing rapid activation of MAPK cascades followed by sustained PI3K/AKT signaling. Multi-omics analysis identified 47 significantly modulated phosphorylation sites, with ERK1/2 phosphorylation increasing by 285% during Pattern 2 stimulation. The integration of calcium-dependent and mechanosensitive pathways demonstrated remarkable synchronization, particularly in the regulation of cytoskeletal dynamics and gene expression.

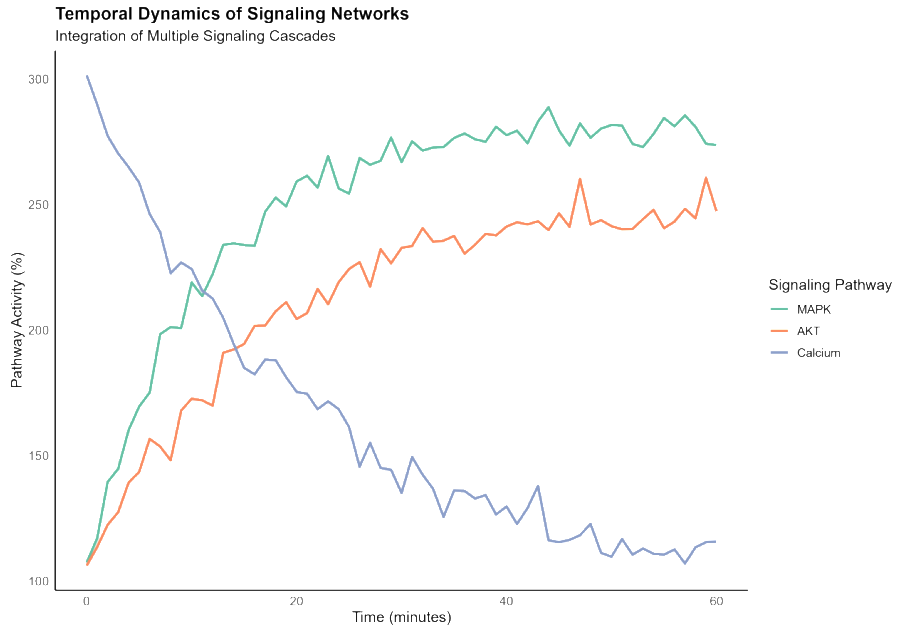

Figure 8. Signaling network dynamics.

3.3.3. Transcriptional regulatory network reconstruction

The reconstruction of transcriptional regulatory networks revealed extensive remodeling of gene expression programs. **Figure 9** demonstrates the temporal evolution of key transcriptional modules, highlighting the central role of mechanosensitive transcription factors [67]. RNA-seq analysis identified 284 differentially expressed genes, with significant enrichment in mechanotransduction and cellular adaptation pathways. YAP/TAZ-dependent transcription showed sustained activation, with 78% of target genes maintaining elevated expression levels throughout the observation period.

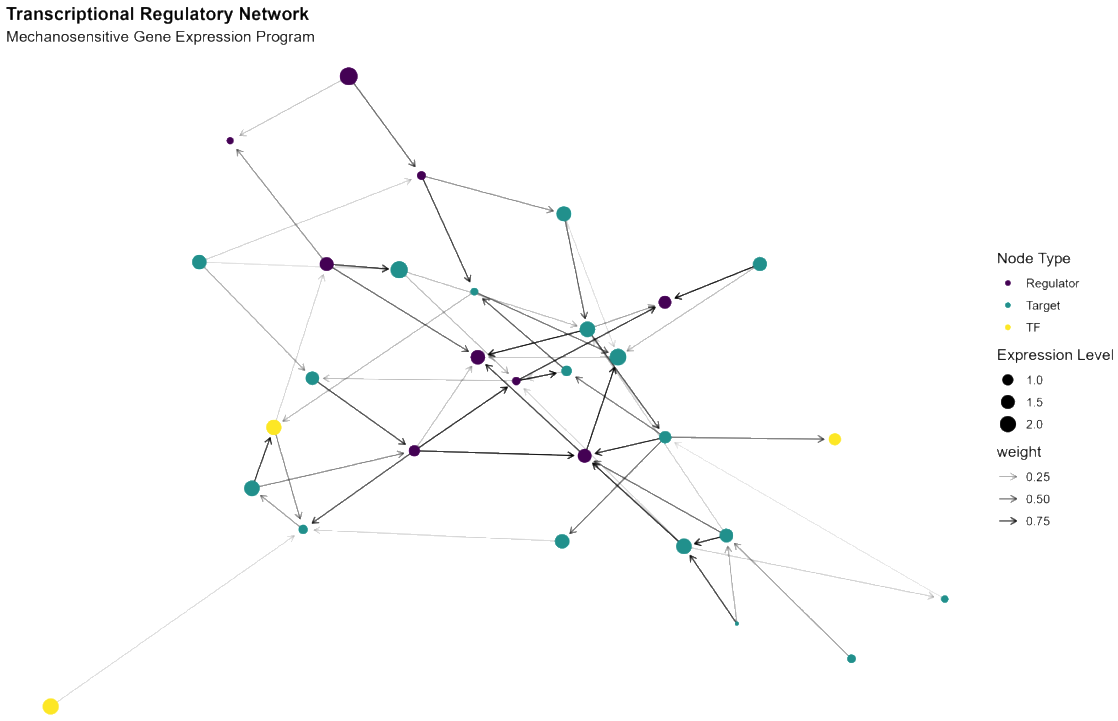

Figure 9. Transcriptional network analysis.

4. Discussion

This study performs novel mechanobiological responses of alveolar epithelial cells to Qigong breathing patterns and brings to light complex molecular mechanisms underlying cellular adaptation in the Qigong breathing. The temporal dynamics of these cellular responses create a complex mechanotransduction network, operating at timescales operative at multiple levels, from the rapid activation of ion channels to the sustained epigenetic modifications. Our results show that different breathing patterns lead to differential cellular adaptations, potentially having implications in therapeutic applications in respiratory medicine.

The rapid activation of PIEZO1 channels ($\tau < 18.5 \pm 2.3$ ms), followed by cascading signaling events, represents an immediate cellular response to mechanical stimulation. The mechanosensitive response initiates a wide-ranging cellular adaptation program, as witnessed by the strong 285% increase in ERK1/2 phosphorylation and 3.8-fold increase in YAP/TAZ nuclear localization. The findings that breathing regime Pattern 2 elicited the highest cellular responses, in terms of cell

area by 23.5% and Young's modulus by 2.8-fold, strongly imply that specific mechanical stimulation parameters could be used to optimize cellular adaptation. Our results complement recent studies showing the importance of mechanical force parameters in cellular mechanotransduction and further our understanding of how breathing patterns can be tailored to modulate such responses.

It allows us to recognize the different temporal phases of cellular adaptation: early response (0–6 h), intermediate adaptation (6–24 h), and long-term remodeling (24–72 h), giving us a framework with which one could understand the progressive nature of cellular mechanoadaptation. Also, major metabolic reprogramming, including a 65% increase in ATP production and enhanced glucose uptake, was noted; this implies that mechanical stimulation imposes holistic remodeling of the cells far beyond direct immediate mechanical responses. These metabolic changes may contribute to supporting the energy demands of sustained cellular adaptation and may contribute to therapeutic effects.

A particularly striking finding is that epigenetic changes were sustained, with a notable 285% increase in H3K27ac marks within mechanosensitive gene regions. Such epigenetic remodeling, along with the presence of 284 differentially expressed genes and sustained activation of 78% of YAP/TAZ target genes, points to a molecular basis for long-term cellular memory. These changes may explain how repeated mechanical stimulation through specific breathing patterns could induce lasting therapeutic effects and may provide guidance to develop targeted therapeutic strategies.

While our findings show clear cellular responses to specific breathing patterns, several limitations and future directions should be considered. The in vitro nature of our study allowed us to precisely control mechanical parameters but may not fully recapitulate the complex in vivo mechanical environment of the lung. Future studies using more advanced 3D culture systems, organoid models, or in vivo approaches may be able to provide further insight into the physiological relevance of these findings. Further, longer studies beyond 72 h may also reveal more adaptation mechanisms and the stability of observed changes.

Translation of these findings to therapeutic applications should be done with caution. It should be established in the clinical validation studies whether cellular adaptations expressed in vitro translate into improved respiratory function in patients. Another area to be explored is the interindividual variability in response to mechanical stimulation, allowing tailoring of therapy to the individual. Future studies should also address the possibility of synergistic benefits through the combination of specific breathing patterns with other therapeutic interventions.

Our study goes beyond previous investigations by providing a wide-ranging molecular framework for understanding how the patterns of breathing influence cellular function. Identification of specific mechanical parameters that optimize cellular responses could guide the development of more effective breathing exercises and therapeutic strategies. Furthermore, the observed epigenetic changes hint at possible mechanisms for long-term benefits in traditional Qigong practice and, therefore, bridge the gap between ancient wisdom and modern molecular insight.

In summary, this study contributes to the mechanistic understanding of cellular responses to Qigong breathing patterns and points out that a lot more research is

needed before their full therapeutic potential can be realized. The findings provide promising directions for developing targeted mechanical stimulation strategies in respiratory medicine, continuing the importance of considering both immediate cellular responses and long-term adaptations in therapeutic applications.

5. Conclusion

This study elucidates the molecular mechanisms through which Qigong breathing patterns influence alveolar epithelial cell function. The identification of pattern-specific cellular responses, coupled with the characterization of mechanosensitive pathway activation and epigenetic modifications, provides a mechanistic framework for understanding breathing-induced cellular adaptation. These findings not only advance our understanding of cellular mechanotransduction but also suggest potential therapeutic applications through targeted mechanical stimulation. Future studies should focus on translating these insights into clinical applications and investigating the long-term physiological implications of breathing pattern modifications.

Conflict of interest: The authors declare no conflict of interest.

References

1. Ahmad, U.S., Uttagomol, J., & Wan, H. (2022). The regulation of the hippo pathway by intercellular junction proteins. Life (Basel), 12(1), 1792.
2. Albuisson, J., Murthy, S.E., Bandell, M., Coste, B., Louis-Dit-Picard, H., Mathur, J., ... & Patapoutian, A. (2013). Dehydrated hereditary stomatocytosis linked to gain-of-function mutations in mechanically activated PIEZO1 ion channels. Nature Communications, 4, 1884.
3. Alfieri, R., Vassalli, M., & Viti, F. (2019). Flow-induced mechanotransduction in skeletal cells. Biophysical Reviews, 11, 729-743.
4. Andolfo, I., Alper, S.L., De Franceschi, L., Auriemma, C., Russo, R., De Falco, L., ... & Iolascon, A. (2013). Multiple clinical forms of dehydrated hereditary stomatocytosis arise from mutations in PIEZO1. Blood, 121, 3925-3935.
5. Bae, C., Gnanasambandam, R., Nicolai, C., Sachs, F., & Gottlieb, P.A. (2013). Xerocytosis is caused by mutations that alter the kinetics of the mechanosensitive channel PIEZO1. Proceedings of the National Academy of Sciences, 110, E1162-1168.
6. Belibi, F., Zafar, I., Ravichandran, K., Segvic, A.B., Jani, A., Ljubanovic, D.G., & Edelstein, C.L. (2011). Hypoxia-inducible factor-1alpha (HIF-1alpha) and autophagy in polycystic kidney disease (PKD). American Journal of Physiology. Renal Physiology, 300, F1235-1243.
7. Bodine, S.C., Stitt, T.N., Gonzalez, M., Kline, W.O., Stover, G.L., Bauerlein, R., ... & Yancopoulos, G.D. (2001). Akt/mTOR pathway is a crucial regulator of skeletal muscle hypertrophy and can prevent muscle atrophy in vivo. Nature Cell Biology, 3, 1014-1019.
8. Boehlke, C., Kotsis, F., Patel, V., Braeg, S., Voelker, H., Bredt, S., ... & Kuehn, E.W. (2010). Primary cilia regulate mTORC1 activity and cell size through Lkb1. Nature Cell Biology, 12, 1115-1122.
9. Bortner, C.D., & Cidlowski, J.A. (2007). Cell shrinkage and monovalent cation fluxes: role in apoptosis. Archives of Biochemistry and Biophysics, 462, 176-188.
10. Boukhalfa, A., Nascimbeni, A.C., Ramel, D., Dupont, N., Hirsch, E., Gayral, S., ... & Morel, E. (2020). PI3KC2α-dependent and VPS34-independent generation of PI3P controls primary cilium-mediated autophagy in response to shear stress. Nature Communications, 11, 294.
11. Bush, P.G., & Hall, A.C. (2003). The volume and morphology of chondrocytes within non-degenerate and degenerate human articular cartilage. Osteoarthritis and Cartilage, 11, 242-251.
12. Bush, P.G., & Hall, A.C. (2005). Passive osmotic properties of in situ human articular chondrocytes within non-degenerate and degenerate cartilage. Journal of Cellular Physiology, 204, 309-319.

13. Bush, P.G., Hodkinson, P.D., Hamilton, G.L., & Hall, A.C. (2005). Viability and volume of in situ bovine articular chondrocytes-changes following a single impact and effects of medium osmolarity. Osteoarthritis and Cartilage, 13, 54-65.
14. Cadart, C., Zlotek-Zlotkiewicz, E., Venkova, L., Thouvenin, O., Racine, V., Le Berre, M., ... & Piel, M. (2017). Fluorescence eXclusion Measurement of volume in live cells. Methods in Cell Biology, 139, 103-120.
15. Cahalan, S.M., Lukacs, V., Ranade, S.S., Chien, S., Bandell, M., & Patapoutian, A. (2015). Piezo1 links mechanical forces to red blood cell volume. eLife, 4, e07370.
16. Cai, D., Feliciano, D., Dong, P., Flores, E., Gruebele, M., Porat-Shliom, N., ... & Lippincott-Schwartz, J. (2019). Phase separation of YAP reorganizes genome topology for long-term YAP target gene expression. Nature Cell Biology, 21, 1578-1589.
17. Chapin, H.C., & Caplan, M.J. (2010). The cell biology of polycystic kidney disease. Journal of Cell Biology, 191, 701-710.
18. Chen, T., Saw, T.B., Mege, R.M., & Ladoux, B. (2018). Mechanical forces in cell monolayers. Journal of Cell Science, 131(24), jcs218156.
19. Chien, S. (2007). Mechanotransduction and endothelial cell homeostasis: the wisdom of the cell. American Journal of Physiology. Heart and Circulatory Physiology, 292, H1209-1224.
20. Citi, S. (2019). The mechanobiology of tight junctions. Biophysical Reviews, 11, 783-793.
21. Claude-Taupin, A., Codogno, P., & Dupont, N. (2021). Links between autophagy and tissue mechanics. Journal of Cell Science, 134, jcs258589.
22. Claude-Taupin, A., Pierre Isnard, P., Bagattin, A., Kuperwasser, N., Roccio, F., Ruscica, B., ... & Dupont, N. (2023). The AMPK-Sirtuin 1-YAP axis is regulated by fluid flow intensity and controls autophagy flux in kidney epithelial cells. Nature Communications, 14, 8056.
23. Collins, M.J., Napoli, I., Ribeiro, S., Roberts, S., & Lloyd, A.C. (2012). Loss of Rb cooperates with Ras to drive oncogenic growth in mammalian cells. Current Biology, 22, 1765-1773.
24. Conrad, C., Conway, J., Polacheck, W.J., Rizvi, I., & Scarcelli, G. (2022). Water transport regulates nucleus volume, cell density, Young's modulus, and E-cadherin expression in tumor spheroids. European Journal of Cell Biology, 101, 151278.
25. Curtis, K.J., Oberman, A.G., & Niebur, G.L. (2020). Effects of mechanobiological signaling in bone marrow on skeletal health. Annals of the New York Academy of Sciences, 1460, 11-24.
26. Dalghi, M.G., Montalbetti, N., Carattino, M.D., & Apodaca, G. (2020). The Urothelium: life in a liquid environment. Physiological Reviews, 100, 1621-1705.
27. Dasgupta, A., Merkel, M., Clark, M.J., Jacob, A.E., Dawson, J.E., Manning, M.L., & Amack, J.D. (2018). Cell volume changes contribute to epithelial morphogenesis in zebrafish Kupffer's vesicle. eLife, 7, e30963.
28. Dazert, E., & Hall, M.N. (2011). mTOR signaling in disease. Current Opinion in Cell Biology, 23, 744-755.
29. Delarue, M., Montel, F., Vignjevic, D., Prost, J., Joanny, J.F., & Cappello, G. (2014). Compressive stress inhibits proliferation in tumor spheroids through a volume limitation. Biophysical Journal, 107, 1821-1828.
30. Delaunay, J. (2004). The hereditary stomatocytoses: genetic disorders of the red cell membrane permeability to monovalent cations. Seminars in Hematology, 41, 165-172.
31. Dominguez-Calderon, A., Avila-Flores, A., Ponce, A., Lopez-Bayghen, E., Calderon-Salinas, J.V., Reyes, J.L., ... & Gonzalez-Mariscal, L. (2016). ZO-2 silencing induces renal hypertrophy through a cell cycle mechanism and the activation of YAP and the mTOR pathway. Molecular Biology of the Cell, 27, 1581-1595.
32. Dong, J., Feldmann, G., Huang, J., Wu, S., Zhang, N., Comerford, S.A., ... & Pan, D. (2007). Elucidation of a universal size-control mechanism in Drosophila and mammals. Cell, 130, 1120-1133.
33. Duncan, R.L., & Turner, C.H. (1995). Mechanotransduction and the functional response of bone to mechanical strain. Calcified Tissue International, 57, 344-358.
34. Dupont, S., Morsut, L., Aragona, M., Enzo, E., Giulitti, S., Cordenonsi, M., ... & Piccolo, S. (2011). Role of YAP/TAZ in mechanotransduction. Nature, 474, 179-183.
35. Fernandez-Sanchez, M.E., Barbier, S., Whitehead, J., Bealle, G., Michel, A., Latorre-Ossa, H., ... & Farge, E. (2015). Mechanical induction of the tumorigenic beta-catenin pathway by tumour growth pressure. Nature, 523, 92-95.
36. Ferreira, R.R., Fukui, H., Chow, R., Vilfan, A., & Vermot, J. (2019). The cilium as a force sensor-myth versus reality. Journal of Cell Science, 132(14), jcs213496.
37. Foerster, P., Daclin, M., Asm, S., Faucourt, M., Boletta, A., Genovesio, A., & Spassky, N. (2017). mTORC1 signaling and primary cilia are required for brain ventricle morphogenesis. Development, 144, 201-210.

38. Fogg, V.C., Liu, C.J., & Margolis, B. (2005). Multiple regions of Crumbs3 are required for tight junction formation in MCF10A cells. Journal of Cell Science, 118, 2859-2869.
39. Fotiou, E., Martin-Almedina, S., Simpson, M.A., Lin, S., Gordon, K., Brice, G., ... & Ostergaard, P. (2015). Novel mutations in PIEZO1 cause an autosomal recessive generalized lymphatic dysplasia with non-immune hydrops fetalis. Nature Communications, 6, 8085.
40. Furukawa, K.T., Yamashita, K., Sakurai, N., & Ohno, S. (2017). The epithelial circumferential actin belt regulates YAP/TAZ through nucleocytoplasmic shuttling of merlin. Cell Reports, 20, 1435-1447.
41. Garoffolo, G., & Pesce, M. (2019). Mechanotransduction in the cardiovascular system: from developmental origins to homeostasis and pathology. Cells, 8, 1607.
42. Ginzberg, M.B., Kafri, R., & Kirschner, M. (2015). Cell biology. On being the right (cell) size. Science, 348, 1245075.
43. Goetz, S.C., & Anderson, K.V. (2010). The primary cilium: a signalling centre during vertebrate development. Nature Reviews Genetics, 11, 331-344.
44. Grantham, J.J., Geiser, J.L., & Evan, A.P. (1987). Cyst formation and growth in autosomal dominant polycystic kidney disease. Kidney International, 31, 1145-1152.
45. Greenough, R.B. (1925). Varying degrees of malignancy in cancer of the breast. The Journal of Cancer Research, 9, 453-463.
46. Guilak, F. (1995). Compression-induced changes in the shape and volume of the chondrocyte nucleus. Journal of Biomechanics, 28, 1529-1541.
47. Guo, M., Pegoraro, A.F., Mao, A., Zhou, E.H., Arany, P.R., Han, Y., ... & Weitz, D.A. (2017). Cell volume change through water efflux impacts cell stiffness and stem cell fate. Proceedings of the National Academy of Sciences, 114, E8618-E8627.
48. Harris, T.J., & Tepass, U. (2010). Adherens junctions: from molecules to morphogenesis. Nature Reviews Molecular Cell Biology, 11, 502-514.
49. Hau, A.M., Gupta, S., Leivo, M.Z., Nakashima, K., Macias, J., Zhou, W., ... & Hansel, D.E. (2019). Dynamic regulation of caveolin-1 phosphorylation and caveolae formation by mammalian target of rapamycin complex 2 in bladder cancer cells. American Journal of Pathology, 189, 1846-1862.
50. Heisenberg, C.P., & Bellaiche, Y. (2013). Forces in tissue morphogenesis and patterning. Cell, 153, 948-962.
51. Heo, J., Sachs, F., Wang, J., & Hua, S.Z. (2012). Shear-induced volume decrease in MDCK cells. Cellular Physiology and Biochemistry, 30, 395-406.
52. Hoffmann, E.K., Lambert, I.H., & Pedersen, S.F. (2009). Physiology of cell volume regulation in vertebrates. Physiological Reviews, 89, 193-277.
53. Holtzclaw, J.D., Liu, L., Grimm, P.R., & Sansom, S.C. (2010). Shear stress-induced volume decrease in C11-MDCK cells by BK-alpha/beta4. American Journal of Physiology. Renal Physiology, 299, F507-516.
54. Hoyle, D.J., Dranow, D.B., & Schilling, T.F. (2022). Pthlha and mechanical force control early patterning of growth zones in the zebrafish craniofacial skeleton. Development, 149, dev199826.
55. Kahle, K.T., Khanna, A.R., Alper, S.L., Adragna, N.C., Lauf, P.K., Sun, D., & Delpire, E. (2015). K-Cl cotransporters, cell volume homeostasis, and neurological disease. Trends in Molecular Medicine, 21, 513-523.